ELSEVIER

Biophysical Chemistry 121 (2006) 105–120

Biophysical Chemistry

http://www.elsevier.com/locate/biophyschem

Orbital based electronic structural signatures of the guanine keto G-7H/G-9H tautomer pair as studied using dual space analysis

D.B. Jones [a], F. Wang [b,*], D.A. Winkler [c,d], M.J. Brunger [a]

[a] *School of Chemistry, Physics and Earth Sciences, Flinders University, GPO Box 2100, Adelaide, SA 5001, Australia*

[b] *Centre for Molecular Simulation and Faculty of Information and Communication Technologies, Swinburne University of Technology, PO Box 218, Hawthorn, Victoria 3122, Australia*

[c] *CSIRO Molecular Science, Private Bag 10, Clayton South MDC, Victoria 3169, Australia*

[d] *School of Chemistry, Monash University, PO Box 23, Victoria 3800, Australia*

Received 13 September 2005; received in revised form 12 December 2005; accepted 12 December 2005
Available online 7 February 2006

Abstract

Electronic structural signatures of the guanine-7H and guanine-9H tautomers have been investigated on an orbital by orbital basis using dual space analysis. A combination of density functional theory (B3LYP/TZVP), the statistical average of model orbital potentials (SAOP/TZ2P) method and outer valence Green's function theory (OVGF/TZVP) has been used to generate optimal tautomer geometries and accurate ionization energy spectra for the guanine tautomer pair. The present work found that the non-planar form for both of the guanine keto pair possesses lower energies than their corresponding planar counterparts, and that the canonical form of the guanine-7H tautomer has slightly lower total energy than guanine-9H. This latter result is in agreement with previous experimental and theoretical findings. In the planar guanine pair the geometric parameters and anisotropic molecular properties are compared, focusing on changes caused by the mobile proton transfer. It is demonstrated that the mobile proton only causes limited disturbance to isotropic properties, such as geometry and the energetics, of the guanine keto tautomer pair. The exception to this general statement is for related local changes such as the $N_{(7)}$–$C_{(8)}$ and $C_{(8)}$–$N_{(9)}$ bond length resonance between the single and double bonds, reflecting the nitrogen atom being bonded with the mobile proton in the tautomers. The mobile proton distorts the electron distribution of the tautomers, which leads to significant changes in the molecular anisotropic properties. The dipole moment of guanine-7H is altered by about a factor of three, from 2.23 to 7.05 D (guanine-9H), and the molecular electrostatic potentials also reflect significant electron charge distortion. The outer valence orbital momentum distributions, which were obtained using the plane wave impulse approximation (PWIA), have demonstrated quantitatively that the outer valence orbitals of the tautomer pair can be divided into three groups. That is orbitals 1a″–7a″ and 18a′, which do not have visible alternations in the tautomeric process (which consist of either π orbitals or are close to the inner valence shell); a second group comprising orbitals 19a′–22a′, 25a′, 26a′, 28a′, 29a′ and 31a′, which show small perturbations as a result of the mobile hydrogen locations; and group three, orbitals 23a′, 24a′, 27a′, 30a′ and 32a′, which demonstrate significant changes due to the mobile proton transfer and are therefore considered as signature orbitals of the G-7H/G-9H keto tautomeric process.

PACS: 31.15.-P
Keywords: DNA bases; Guanine; Tautomers; Dual space analysis; Structural signatures

1. Introduction

The demand for gas phase information, which arises from the anticipation that many biological phenomena can be traced to the fundamental properties of their molecular constituents, has led to an outburst of research interest in small biological molecules in the gas phase in recent years [1–3]. The intrinsic properties of these molecules, which are usually hidden in the complex medium of a real biological system, can be understood in an isolated environment. Both laser spectroscopy and computational modeling have contributed significantly to elucidating the structures and dynamics of these biomolecules, and their solvated complexes in the gas phase [1,3,4]. For

* Corresponding author. Tel.: +61 3 9214 5065; fax: +61 3 9214 5075.
E-mail address: fwang@swin.edu.au (F. Wang).

0301-4622/$ - see front matter © 2006 Elsevier B.V. All rights reserved.
doi:10.1016/j.bpc.2005.12.006

example, the flexible single bonds of glycine are responsible for the conformational changes in side chains of many proteins. On the other hand, an earlier electron momentum spectroscopic study of glycine [4] added significant momentum space information towards our understanding of its fundamental structure. Moreover, a recent experiment using the resonant two photon ionization (R2PI) technique revealed that the ionization energy of an aromatic amino acid (phenylalanine) was conformer dependent [1]. Tautomerism due to the mobile proton shift is largely engaged with DNA bases such as guanine. As an understanding of tautomerism in DNA bases is fundamental to characterizing any potential damage to DNA, and is vital for understanding its chemical reactivity, a tautomer cannot be ignored even if it is a minor one [5].

Guanine ($C_5N_5H_5O$) is one of the biologically important purines, which together with the pyrimidines form the bases for RNA and DNA. It has already been identified as a target site for carcinogens and a receptor site for anticancer drugs. In addition it is also involved in the activation of enzymes [6,7], which has made it the subject of many recent studies [8–10]. One such recent study indicated [11] that guanine serves as the reducing agent in DNA, making it a favored site for oxidation and DNA damage. Although only a medium-sized molecule (with 78 electrons), guanine is the most challenging of the DNA bases being larger in size when compared to the other DNA/RNA bases. This challenge is heightened by its many possible tautomers and isomers, such as keto (C═O), –enol (C–OH), amino (–NH_2) and –imino (–NH) as well as the prototypic tautomers such as N1H–N3H and N7H–N9H. These guanine tautomers are very close in energy [12] and result in as many as 15 different tautomeric forms [13], in addition to the non-planar structures. Some of the guanine tautomers in the gas phase, such as the keto pair of guanine-7H (G-7H) and guanine-9H (G-9H), and the enol G-7H and G-9H pair, have been identified experimentally with near UV spectroscopy [14], IR–UV spectroscopy [15] and in gas phase by photoelectron spectroscopy (PES) [16,17]. Discrepancies in the assignment of the various spectral lines have been reported, due to the spectrum being composed of a superposition of vibrational spectra from multiple tautomers. It is therefore essential that theoretically calculated energy parameters are determined as accurately as possible, in order to enhance the interpretation of the experimental results.

The stability of the various tautomers is difficult to determine experimentally as the bases, with small energy differences, are difficult to isolate. Hence theoretical studies of tautomers using accurate quantum mechanical calculations have played an important role [18,19] in this respect. In recent studies, the energies of the respective guanine tautomers have been shown to be sensitive to the model chemistry and basis set employed in the calculations, with the energy ordering of the tautomers changing between the different calculations [20]. The G-9H and G-7H tautomers (see Fig. 1) are consistently the lowest energy pair, although the lower energy tautomer in this pair alters between the different model chemistries [12]. Planarity of the DNA base has been another area of previous studies [18,19]. Early investigations indicated that the isolated guanine molecule was planar, whilst more recent studies have shown that there is a substantial pyramidalization in the amine group [21]. There is therefore a need to explore new and more sensitive techniques, both experimental and theoretical, to assist in distinguishing between the tautomer subtle electronic structures and in so doing, rationalizing their behaviors in response to different chemical environments and reactions. As it has previously been successful in identifying structural signatures in adenine tautomers [22], the dual space analysis (DSA) technique [23] will now be applied in this study to investigate the guanine tautomers.

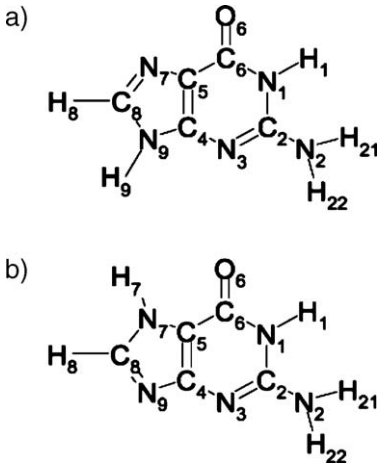

Fig. 1. Schematic structures of (a) G-9H and (b) G-7H.

In the next section of this paper, a brief outline of the computational details pertaining to DSA, including generation of orbital momentum distributions, is provided. Thereafter, in the results and discussion section, comparisons are made between the tautomer pair through their respective geometries, non-planarity, stabilities, anisotropic properties such as dipole moments, molecular electrostatic potentials, binding energy spectra and momentum distributions on an orbital by orbital basis. Finally, we present the important conclusions drawn from this study.

2. Method and computational details

The atomic numbering systems of the G-9H and G-7H tautomer pair are given in Fig. 1. The purine ring of the species is oriented in the *xy*-plane. The *x*-axis is along the $N_{(1)}$–$C_{(2)}$ bond. Quantum mechanical calculations employed in the present work use the B3LYP [24,25] hybrid three parameter electron correlation-exchange functional, V_{xc}, together with the DGauss triple zeta valence polarized (TZVP) basis set of Godbout et al. [26]. The electronic calculations of the guanine tautomers were performed using the Gaussian 03 computational chemistry package [27]. This combination of model chemistry and basis set, has previously proved reliable for generating orbital momentum distributions [28–31] and so is employed again here.

The accuracy of orbital energies obtained through density functional theory (DFT) methods, has traditionally been found to be in poor agreement with experimental photoelectron spectroscopy (PES) and electron momentum spectroscopy

(EMS) binding energy measurements. This is because Koopmans' theorem [32] does not hold for Kohn–Sham orbital energies in the independent particle picture. We therefore performed supplementary calculations using the outer-valence Greens Function (OVGF) theory [33,34] and the recently developed orbital dependent statistical average of different model orbital potentials (SAOP) [35–37] method. This latter approach is undertaken within a DFT framework, and it provides accurate binding energies [38,39]. The OVGF model is embedded in the Gaussian 03 package [27], whereas the SAOP model is embedded in the Amsterdam Density Functional (ADF) suite of programs [40]. The present SAOP calculations employ the TZ2P basis set, which is a Slater type triple zeta basis set with double polarization [41], and is the closest basis set to the Gaussian TZVP basis set [26] employed in our other calculations. Note that the OVGF and SAOP calculations have been performed at the B3LYP/TZVP optimized geometries.

Orbital momentum distributions (MDs) are obtained from a theory [42] which employs the Born–Oppenheimer, independent particle and plane wave impulse approximations (PWIA). Here the EMS cross section [42] for randomly oriented molecules is given by

$$\sigma = K \int \mathrm{d}\Omega |\langle p \Psi_f^{N-1} | \Psi_i^N \rangle|^2, \quad (1)$$

where K is a kinematical factor (which is approximately constant for EMS symmetric non-coplanar conditions), Ψ_f^{N-1} is the residual ion $N-1$ electron many-body wave function, Ψ_i^N is the N electron many-body ground state wave function and p is a plane wave. Here the integration performs the spherical averaging over the initial rotational states. We also note that the averaging over initial vibrational states is incorporated by considering the orbitals at the molecular equilibrium geometry, whilst closure eliminates the final rotational and vibrational state dependence [42]. The overlap between the ion and target, is a one electron orbital known as the Dyson spin-orbital. This can be approximated by the molecular orbital (MO), $\phi_j(p)$, in the weak coupling approximation. The cross section in Eq. (1) then becomes

$$\sigma = K S_j^{(f)} \int \mathrm{d}\Omega \mid \phi_j(p)|^2, \quad (2)$$

where the spectroscopic pole strength, $S_j^{(f)}$, is the probability of finding the one-electron hole configuration in the final ion many-body wave function and p is now the momentum of the target electron at the instant of ionization. For symmetric non-coplanar kinematic conditions, the MDs are measured as a function of azimuthal angle, ϕ, which is equivalent to changing the momentum, p, as

$$p = \left[(2k_s \cos\theta - k_0)^2 + 4k_s^2 \sin^2\theta \sin^2\left(\frac{\phi}{2}\right) \right]^{\frac{1}{2}}, \quad (3)$$

where k_0 and k_s are the momenta of the incident and scattered electrons, respectively, and θ is the polar angle, which is held constant ($\theta = 45°$). The implementation of this method is carried out in the AMOLD codes of McCarthy and Weigold [43], where we employ the same kinematic parameters as those typically used in the Flinders University based high resolution electron momentum spectroscopy spectrometer [44]. A recent EMS measurement on N_2O, at different impact energies, indicated that the MDs of all its orbitals did not show variations with impact energy (when the impact energy is sufficiently high), thereby confirming the validity of the PWIA [45].

As the orbital MD calculations employ the independent particle approximation, the electron propagator calculations generate pole strengths (PS) to indicate if the one-electron model is appropriate for the individual orbitals. Here we note that generally the one electron picture is valid for PS greater than 0.85 [46], i.e., that particular orbital dominates the configuration of the final state. Together with a qualitative visualization of the orbital charge density distributions, the orbital MDs provide quantitative information into the chemical bonding mechanism of a species. The low momentum (or small azimuthal angle) region provides information on the long range behavior of the orbital wave function, the accuracy of which is not usually automatically guaranteed by quantum chemistry [43]. If the orbital MD possesses a maximum intensity at zero momentum, this orbital is likely to be dominated by contributions from *s*-electrons, which is particularly true in atoms. Conversely, *p*-electrons exhibit a Gaussian-like distribution in which the orbital MDs are small (nearly zero) in the small momentum region before increasing as momentum increases, to a maximum and then decreasing again at large momentum. In molecules, the orbital MD shapes are often distorted as a result of chemical bonding and sp hybridization [28]. However, if the component atoms of a molecule are from the first row of the periodic table, such as with the DNA bases, their valence orbitals are dominated by *p* electrons, with the effects of electrons from higher angular momentum orbitals such as *d*-, *f*-,... etc. being negligible. One can, therefore, comment on the bonding nature of molecular orbitals based on the shape of the orbital MDs. As guanine only contains C, N, O and H atoms, there are just minimal contributions from the *d*-, *f*-,... electrons. As a result, orbital contributions from atomic orbitals with non-zero angular momentum can be attributed to *p*-electrons. Since we are dealing with molecular orbitals, the notation '*s*-like' is used to indicate that the MO is dominated by *s*-electrons, '*p*-like', is used to indicate that the MO is dominated by *p*-electrons, and 'hybrid-like' is used to describe MOs with mixed contributions from *s*- and *p*-electrons.

In this study, we will briefly discuss the non-planarity of the guanine tautomers and their implication to the molecular structures. However, the focus will be placed on the planar guanine tautomer pair, as the increased symmetry assists with the orbital classifications. For planar molecules, the a″ symmetry molecular orbitals, which possess an anti-symmetrical reflection about the molecular plane, are likely to form π-bonds produced by the overlap of the $2p_z$-atomic orbitals (AOs). The MOs of a″ symmetry should thus be less affected by the in-plane proton transfer between $N_{(7)}$ and $N_{(9)}$, and therefore are unlikely to contain any prototype tautomeric signature information (see later).

3. Results and discussion

3.1. Geometry, non-planarity and stability

The ground electronic states (X^1A') of the G-7H and G-9H tautomers each consist of a closed shell, with 39 doubly occupied MOs. Total electronic energies of the tautomers, either planar or non-planar, which are obtained from optimization at the B3LYP/TZVP model, are given in Table 1. The keto tautomers, either in C_s (planar) or C_1 (non-planar) symmetry, are extremely close in energy. In fact, the non-planar keto guanine pair exhibit lower total energies than their planar counterparts, indicating that both the G-7H and G-9H keto tautomers energetically prefer a non-planar form rather than planar configurations. Moreover, regardless of the planarity, the tautomer with the mobile proton at the $N_{(7)}$ position represents the global minimum, whereas the canonical form of G-9H with the mobile proton locating on the $N_{(9)}$ position represents a local minimum. Such a result agrees with the findings of Hanus et al. [8], using a variety of theoretical models [20,8,47] including the RI-MP2/TZVPP [48] and CCSD(T) models and which include zero-point energy (ZPE) and temperature-dependent enthalpy terms and entropies [8]. The photoelectron spectroscopy (PES) [16,17] and IR spectroscopy [49] experiments indicated that the keto G-7H tautomer was slightly more abundant. The energy difference between the planar G-7H and G-9H forms is only 0.44 kcal mol^{-1}, as given in the present study, which also agrees well with the value of 0.50 kcal mol^{-1} from the RI-MP2/TZVPP model [8]. However, we note that some previous calculations [15,50,7] predicted an opposite stability order for the keto guanine pair. Nevertheless, what is in agreement among the various models is that the energy difference between the keto G-7H and G-9H tautomers is smaller than 1.0 kcal mol^{-1} [8,50].

All the available experiments, such as UV–UV and IR–UV spectroscopy [15], which identify the guanine tautomers, are unable to indicate the stability order amongst them. This is especially true for the ones which are very close in energy. Theoretically, the energy differences among some of the tautomers are so small that the resultant energy alterations, as caused by the tautomerism, are within the errors introduced by the model chemistry employed. For example the basis set superposition error (BSSE) could be as high as 3.88 kcal mol^{-1}, using the MP2/6-311++G(p,d)//HF/6-311G(d,p) model, in a study of the guanine–cytosine pair interaction [51], even though the BSSE is generally larger in inter-molecular interactions than intra-molecular interactions. As a result, to draw definitive conclusions on the stability of tautomers with an energy difference smaller than the possible model errors would not be a meaningful exercise. This reality also indicates that the energetic and largely isotropic molecular properties may not be the most appropriate means (candidates) for the study of tautomerism. Therefore, it is important to explore other properties which might be more sensitive to reflect changes in the position of the mobile protons. These properties can be either anisotropic properties such as the dipole moment, molecular electrostatic potentials (MEPs) and molecular orbital charge distributions in coordinate space, or orbital based electronic information such as the orbital momentum distributions (MDs).

The optimized geometries for the keto guanine pair using the B3LYP/TZVP model are reported in Table 2. These data are compared against a number of previously calculated values, and a statistical analysis of experimental X-ray and neutron crystal structure measurements, for the geometry of G-9H [52]. Comparing the geometric parameters in G-9H, there is generally good overall agreement between the different theoretical models, except for the $N_{(7)}$–$C_{(8)}$ bond length where the calculated value from perturbation theory (RI-MP2) is significantly greater than those calculated using our model and the experimental measurement. On further comparison with experiment, it is noted that the theoretical values for the double bonds in G-9H, i.e., $C_{(2)}{=}N_{(3)}$ and $C_{(6)}-O_{(6)}$ are apparently shorter than those from the experimental measurements. Conversely, the predicted values for other bonds in G-9H, that is the $C_{(4)}{=}C_{(5)}$, $C_{(5)}$–$C_{(6)}$ and $N_{(1)}-C_{(6)}$ bond lengths, are substantially longer than the corresponding experimental values. Apart from possible intrinsic errors introduced in the models, discrepancies between theoretically predicted bond lengths and the experimentally observed values indicate a resonance of the guanine tautomers. This has been observed recently in a UV spectrum [14] and with UV–UV and IR–UV spectroscopies [15]. Due to proton affinity of nitrogen atoms, the mobile proton is able to land on different nitrogen atoms in the purine ring of guanine, which results in prototypic tautomerism, i.e., the keto forms. In addition the hydrogen atom at the $N_{(1)}$ position can also relocate to the oxygen atom to form a hydroxyl group, which results in the C=O double bond reducing to a C–OH single bond. Such tautomeric processes lead to simultaneous equilibria of single bonds ⇔ double bonds. As a consequence the experimental results for the guanine bond lengths are the averaged bond lengths of many tautomers, which exist under the experimental conditions. This was previously observed in our study of *cis*-1,3-butadiene/gauche-1,3-butadiene [53]. For G-7H, we note that there is quite good agreement observed between the present calculations for bond lengths and

Table 1
Guanine tautomer energies and dipole moments, calculated at the B3LYP/TZVP//B3LYP/TZVP level

Molecule	E_{ZPE} (kcal mol^{-1})	$E=\Sigma(E_{Elec}+E_{ZPE})$ (E_h)	ΔE (kcal mol^{-1})	μ_x (D)	μ_y (D)	μ_z (D)	μ (D)
G-7H	73.03	−542.604724	0.00	−0.61	−1.49	−0.87	1.83
G-7H (Planar)	72.35	−542.604658	0.04	−0.52	−2.17	0.00	2.23
G-9H	72.93	−542.604021	0.44	6.28	−2.42	−0.80	6.78
G-9H (Planar)	72.30	−542.603868	0.54	6.38	−3.01	0.00	7.06

Refer to Fig. 1 for tautomer labelling. The energy difference (ΔE) is calculated with respect to the guanine-7H tautomer energy.

Table 2
The optimized theoretical and experimental bond lengths (Å), bond angles (°) and dihedral angles (°) for the G-7H and G-9H tautomers

Parameter	G-7H	G-7H	G-7H	G-7H	G-9H	G-9H	G-9H	G-9H	G-9H
	B3LYP/	B3LYP/	RI-MP2/	B3LYP/	B3LYP/	B3LYP/	RI-MP2/	B3LYP/	Expt.
	TZVP	TZVP	TZVPP	cc-pVDZ[a]	TZVP	TZVP	TZVPP	cc-pVDZ[a]	[52]
		(planar)	[8]	[57]		(planar)	[8]	[57]	
Bond lengths (Å)									
$N_{(1)}C_{(2)}$	1.381	1.381	1.378	1.382	1.370	1.371	1.366	1.371	1.371
$C_{(2)}N_{(3)}$	1.302	1.305	1.297	1.306	1.309	1.311	1.304	1.314	1.324
$N_{(3)}C_{(4)}$	1.366	1.363	1.384	1.369	1.357	1.355	1.360	1.360	1.351
$C_{(4)}C_{(5)}$	1.392	1.393	1.407	1.398	1.391	1.392	1.392	1.398	1.378
$C_{(5)}C_{(6)}$	1.422	1.420	1.428	1.430	1.436	1.435	1.439	1.444	1.418
$C_{(5)}N_{(7)}$	1.379	1.381	1.362	1.379	1.382	1.383	1.373	1.383	1.388
$N_{(7)}C_{(8)}$	1.364	1.363	1.365	1.365	1.306	1.305	1.319	1.310	1.304
$C_{(8)}N_{(9)}$	1.319	1.319	1.322	1.323	1.385	1.386	1.371	1.386	1.373
$C_{(6)}O_{(6)}$	1.228	1.228	1.224	1.225	1.219	1.219	1.216	1.217	1.238
$N_{(1)}H_{(1)}$	1.012	1.012	1.011		1.012	1.012	1.011		
$C_{(2)}N_{(2)}$	1.381	1.365	1.384	1.385	1.377	1.363	1.379	1.380	1.377
$N_{(2)}H_{(21)}$	1.010	1.003	1.008		1.009	1.003	1.007		
$N_{(2)}H_{(22)}$	1.010	1.006	1.206		1.010	1.005	1.008		
$C_{(8)}H_{(8)}$	1.079	1.079	1.077		1.079	1.079	1.076		
$N_{(7)}H_{(7)}$	1.008	1.008	1.007						
$N_{(9)}H_{(9)}$					1.008	1.008	1.006		
$N_{(1)}C_{(6)}$	1.418	1.420	1.404	1.420	1.439	1.439	1.425	1.440	1.391
$C_{(4)}N_{(9)}$	1.373	1.374	1.378	1.375	1.370	1.370	1.366	1.371	1.374
$\bar{R}_5$	6.827	6.830	6.835	6.840	6.834	6.836	6.821	6.848	6.817
$\bar{R}_6$	8.280	8.282	8.298	8.305	8.302	8.303	8.286	8.327	8.233
Bond angles									
$N_{(1)}C_{(2)}N_{(3)}$	124.1	124.0	124.8	124.6	123.4	123.2	123.9	123.7	123.7
$C_{(2)}N_{(3)}C_{(4)}$	114.5	114.5	113.4	114.1	112.8	112.8	111.8	112.3	112.0
$N_{(3)}C_{(4)}C_{(5)}$	124.2	124.4	121.9	124.3	129.1	129.2	129.5	129.4	128.7
$C_{(4)}C_{(5)}N_{(7)}$	105.7	105.8	105.6	105.6	110.8	110.8	111.4	111.0	110.8
$C_{(5)}N_{(7)}C_{(8)}$	106.0	106.0	106.3	106.1	104.8	104.9	104.0	104.5	104.4
$H_{(1)}N_{(1)}C_{(2)}$	120.1	120.6	119.1		120.0	120.4	119.2		
$N_{(2)}C_{(2)}N_{(1)}$	115.9	116.5	114.8		117.0	117.4	116.1		116.4
$C_{(2)}N_{(2)}H_{(21)}$	117.3	123.3	115.0		117.9	122.9	115.8		
$C_{(2)}N_{(2)}H_{(22)}$	112.3	117.3	105.6		113.4	117.7	111.7		
$N_{(1)}C_{(6)}O_{(6)}$	121.2	121.0	122.2		119.1	118.9	119.9	119.2	120.0
$N_{(7)}C_{(8)}H_{(8)}$	121.9	121.8	121.8		125.7	125.7	125.3		
$C_{(5)}N_{(7)}H_{(7)}$	126.1	126.1	126.0		125.6	125.6	125.6		
$C_{(6)}N_{(1)}C_{(2)}$	125.2	125.2	125.8		126.4	126.4	127.1	126.7	125.1
$N_{(9)}C_{(4)}N_{(3)}$	125.6	125.5	123.3		125.8	125.8	125.7		125.9
$N_{(9)}C_{(4)}C_{(5)}$	110.2	110.1	108.9	110.4	105.1	105.0	104.8	104.9	105.4
$C_{(4)}C_{(5)}C_{(6)}$	122.8	122.7	122.7	122.9	118.8	118.7	118.6	118.6	118.8
$C_{(4)}N_{(9)}C_{(8)}$	104.9	104.9	104.4		106.7	106.7	107.0	106.7	106.4
Dihedral angles									
$C_{(4)}N_{(3)}C_{(2)}N_{(1)}$	0.9		9.7		0.9		0.9		
$C_{(5)}C_{(4)}N_{(3)}C_{(2)}$	−1.5		−19.5		−1.3		−1.3		
$C_{(6)}N_{(1)}C_{(2)}N_{(3)}$	−0.1		0.0		−0.3		−0.3		
$N_{(7)}C_{(5)}C_{(4)}N_{(3)}$	−179.5		−167.3		−179.4		−179.5		
$C_{(8)}N_{(7)}C_{(5)}C_{(4)}$	0.1		8.2		0.1		0.1		
$N_{(9)}C_{(4)}N_{(3)}C_{(2)}$	179.2		−169.4		179.5		179.4		
$N_{(2)}C_{(2)}N_{(1)}C_{(6)}$	177.2		176.7		177.2		176.6		
$O_{(6)}C_{(6)}N_{(1)}C_{(2)}$	−179.6		−179.7		−179.7		−179.7		
$H_{(7)}C_{(7)}C_{(5)}C_{(4)}$	−179.7		−171.6						
$H_{(8)}C_{(8)}N_{(7)}C_{(5)}$	179.9		180.0		180.0		−179.9		
$H_{(9)}N_{(9)}C_{(4)}C_{(3)}$					−0.7		−0.2		
$H_{(21)}N_{(2)}C_{(2)}N_{(1)}$	36.7		44.4	43.1	32.2		38.2	36.2	
$H_{(22)}N_{(2)}C_{(2)}N_{(1)}$	171.2		144.8	167.5	169.8		169.3	165.7	
$H_{(1)}N_{(1)}C_{(2)}N_{(3)}$	−174.9		−174.7		−175.9		−175.9		

See Fig. 1 for the atom labelling.
[a] The geometry is planar, with a non-planar amino group.

bond angles and those from previous studies for the planar tautomer pair.

The geometric parameters, in particular the bond lengths, of the keto G-7H/G-9H tautomers, almost remain unchanged regardless of whether it is the G-7H/G-9H tautomer or C_s/C_1 symmetry. The bond lengths between the planar and non-planar species of the same tautomer also receive only small perturbations, which has been observed in the pentagonal and hexagonal ring lengths, $\overline{R}_5$ and $\overline{R}_6$ (perimeters), as introduced by Wang et al. [22]. For example, we see from Table 2 that the G-7H pentagonal ring lengths are 6.827 and 6.830 Å for the C_1 and C_s configurations, respectively, whereas the hexagonal ring lengths of the pair are respectively given by 8.280 and 8.282 Å. The overall "backbone" bond length changes for the C_1 and C_s symmetries are thus less than 0.003 Å for both rings of G-7H. The alternation in bond lengths due to the non-planarity is even smaller in the G-9H case, as can also be seen in the same table. For the bond angles, again, the C_1 and C_s related changes are very small and in general, within 1.0° for the majority of angles. The exception to this is for the amine group related angles which are discussed next. The dihedral angles of the C_1 structures of G-7H and G-9H indicate small relaxations in almost the same way: for example, the $C_{(4)}$–$N_{(3)}$–$C_{(2)}$–$N_{(1)}$ dihedral angle changes 0.9° when guanine experiences C_1/C_s changes, which is true for both G-7H and G-9H.

The most significant non-planarity observed in comparison with their planar counterparts, of G-7H and G-9H, is due to the pyramidalization of the amine group and the proton bonding to $N_{(1)}$ being slightly out of plane. In addition, a small degree of purine ring relaxation has been observed in the non-planar configurations of both the G-7H and G-9H tautomers. The non-planarity of G-7H and G-9H is caused by the interaction between the hydrogen atom positioned on the $N_{(1)}$ atom and the closer hydrogen atom, $H_{(21)}$, in the amine group. This interaction also results in the $H_{(21)}$ atom tipping over to the other side of the $–NH_2$ group, in order to accommodate the interaction. Hence, the amine group loses its local symmetry of C_{2v}. In Table 2, it is also seen that the pyramidalization effect of the amine group is less significant in G-9H than in G-7H, since in G-9H the mobile proton on $N_{(9)}$ may have a stronger "throughbond" interaction with the amine group to compensate for the changes caused by $N_{(1)}$–H from the other side of the amine group. This follows as the $N_{(9)}$–H position in G-9H is closer to the amine group in the purine ring than in the G-7H tautomer. For example, the $H_{(21)}N_{(2)}C_{(2)}N_{(1)}/H_{(22)}N_{(2)}C_{(2)}N_{(1)}$ angle pair of $–NH_2$ is 36.7°/8.8° (absolute values) for non-planar G-7H, whereas this pair yields a ratio of 32.2°/10.2° for non-planar G-9H. Similar angle ratios of the amine group have also been found in the adenine amino tautomer of A-7H (32.5°/11.1°) [21]. The angle ratios of the guanine G-7H/G-9H pair exhibit the same trend of $H_{(21)}N_{(2)}C_{(2)}N_{(1)} > H_{(22)}N_{(2)}C_{(2)}N_{(1)}$, since only the hydrogen atom bonding with the $N_{(1)}$ position directly interacts with the $H_{(21)}$ of the amine group and it is this which tips this hydrogen atom ($H_{(21)}$) out of the plane. The non-planarity of G-7H and G-9H is also evident in their corresponding dipole moments in the out-of-plane *z*-direction. For example, μ_z is −0.8664 and −0.7978 D for the G-7H and G-9H non-planar tautomers, respectively, as indicated in Table 1. These μ_z components contribute to a reduction in the total dipole moments compared to their planar counterparts, since the non-planarity relaxes the planar structure to produce a non-zero dipole moment in the out-of-plane *z*-direction.

3.2. Anisotropic properties

The total electronic energy and geometric configuration between the planar and non-planar molecules are extremely close, so that changes due to the proton transfer are more profound than confinement to a plane, unless the pyramidalization of the amine group is particularly important. The present study therefore now analyzes the behavior of the prototypic tautomerism of planar guanine molecules, which may also be leveraged in a study of tautomerism in the purine ring of their C_1 counterparts, by considering some of their anisotropic properties.

Prototypic tautomerism does not significantly affect isotropic properties, such as geometry and total energies, as demonstrated in the previous section. However, the location of the mobile proton certainly changes the electron charge distributions of the species, which results in changes in the tautomer anisotropic properties. These changes are reflected in the dipole moment, electrostatic potentials and the shape of the valence orbital MDs. The mobile proton transfer, between the $N_{(7)}$ and $N_{(9)}$ positions, results in a significant change (>×3) in the dipole moment. For example the dipole moments for planar G-7H and G-9H are 1.83 and 6.78 D, respectively (see Table 1), which may be considered as a structural signature of G-9H. Therefore, the G-9H tautomer may behave very differently in aqueous solutions than in gas phase. Such a significant change in the dipole moment has also been previously observed in the adenine amino tautomer pair of A-7H and A-9H. However, in that case A-7H had a larger dipole moment than that of the canonical A-9H tautomer [22]. Nonetheless, the reasons underlining the differences between the dipole moments of the pairs are similar: it is dependent on the relative position of the mobile H and the amine group. Due to convention, in adenine the $C_{(6)}$ position bonds with the N atom of the $–NH_2$ group, which locates at the upper part of the hexagonal ring (HU), while the $N_{(7)}$–H proton locates in the upper part of the pentagonal ring (PU). The latter enhances the polarity of the molecule, so that the HU–PU configuration leads to an increase in the dipole moment of A-7H. In A-9H, on the other hand, the $N_{(9)}$–H proton positions itself in the lower part of the pentagonal ring (PL). The resultant HU–PL configuration helps to balance the charge polarity and leads to a smaller dipole moment for A-9H. In guanine, the $C_{(6)}$ position bonds with the O atom (HU) for the keto configuration, whereas the amine group locates on an HL position of $C_{(2)}$. If the mobile proton bonds with $N_{(7)}$ (PU) in G-7H, the PU–HL configuration helps balance the electron distribution, while in G-9H the mobile proton bonds with $N_{(9)}$ (PL), so that the HL–PL configuration enhances the polarity of the species, and hence enlarges the dipole moment in G-9H. Comparing to the adenine counterparts, whose dipole moments are 2.44 and 7.38 D for A-9H and

A-7H respectively, the dipole moments for the guanine G-9H/G-7H pair are given by 6.78/1.83 D using the same model of B3LYP/TZVP. Due to the keto C═O group in guanine being in the HU position, this contributes to reduce the polarity of the species.

Fig. 2 gives the molecular electrostatic potentials (MEPs) of the guanine keto tautomer pair. As expected, the oxygen atom in the tautomers attracts intensive negative charge in both the G-7H and G-9H cases, as do the "bare" nitrogen atoms such as $N_{(3)}$ and $N_{(9)}$ in G-7H and $N_{(3)}$ and $N_{(7)}$ in G-9H. In addition, the pentagonal ring in both cases exhibits negative charge and the hexagonal ring exhibits positive charge. The positive charge centered on the proton of $N_{(1)}$ and $H_{(21)}$ of the $-NH_2$ group, exhibits noticeable repulsive forces which, as observed before, tips the $H_{(21)}$ atom over. The negative charge centered on the O and N atoms results from the contributions of the lone pair of electrons residing on the atoms in both tautomers. However, while the distribution of the positive charges in G-7H and G-9H are not very different, the concentration of the negative charges is more evenly balanced in the G-7H configuration than for the G-9H case. Other positive charges, such as protons, could form hydrogen bonds with G-9H easily. Therefore, it would not be surprising if the rarer but less stable tautomers in the gas phase could be dramatically stabilized in polar solutions such as water [8], or by other nucleic bases [9]. Moreover, the MEPs of G-7H and G-9H indicate that negative charge deposits are more concentrated on the "bare" nitrogen atom in the pentagonal ring, $N_{(9)}$ and $N_{(7)}$ in G-7H and G-9H, respectively. This contributes to the overall negative charge deposits in the pentagonal ring and as a consequence, the next protonation position of the guanine pair can be expected to be a H-bond on the "bare" nitrogen position in the pentagonal ring [54].

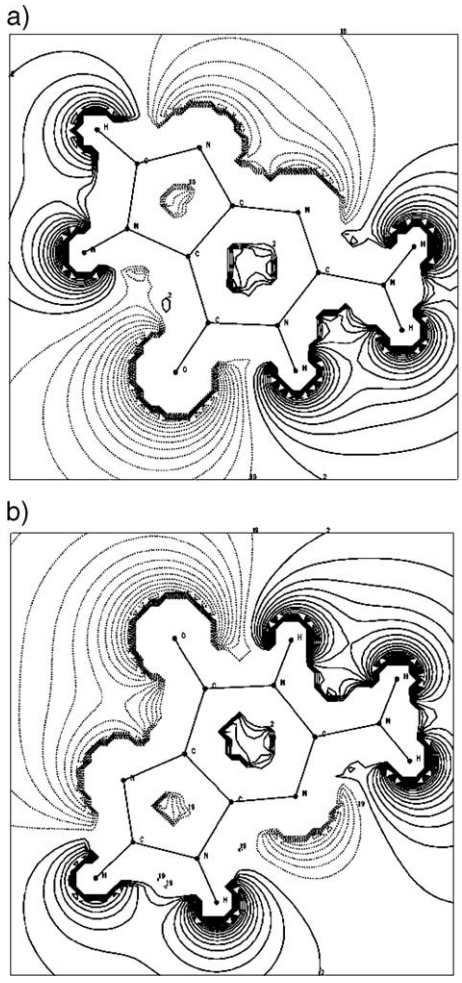

Fig. 2. The molecular electrostatic potentials for (a) G-7H and (b) G-9H calculated at the B3LYP/TZVP level.

3.3. Binding energy spectra

The ionization of nucleotides play important roles in the chemistry and biology of DNA. In most cases guanine has either been found to be the initial oxidation site, or the electron loss center ultimately moves through the DNA π stack to end up at a guanine base [55]. This is attributed to the low (first) ionization potential (IP) of guanine relative to other DNA bases, and has been recognized as a fingerprint of guanine [11] (in relation to other DNA bases). However to understand the experimental findings from, e.g. photoelectron spectroscopy, a detailed understanding of the molecular electronic structure, at least in the valence space is required. In particular, calculating the first ionization energy of a species is not sufficient for an understanding of the electronic structure of the entire molecule. This follows because the tautomeric changes to molecular properties are more or less bond (or orbital) dependent, since this information is contained in the wave functions. We therefore proceed to study the valence orbitals of the guanine tautomer pair in more detail. The valence space binding (ionization) energy spectra and their associated Dyson orbitals are consequently discussed in the remainder of this section.

The guanine keto G-7H/G-9H tautomer pair each have a closed shell with 39 doubly occupied molecular orbitals (MOs), including 17 outer valence MOs in the binding energy region $\epsilon_j < 20$ eV. Table 3 reports the MO binding energies determined for the planar and non-planar G-7H and G-9H tautomers, respectively, under the independent particle picture. A comparison is also made (where possible) against the results from other calculations and available experiments in this table. Good agreement is achieved between the two electron propagator calculations, i.e. the partial third order approximation (P3) technique [50] and the present OVGF/TZVP model, which both also agree well with the available PES experimental results for G-7H. Similarly, good agreement between the P3 calculations [50] and our OVGF/TZVP result for G-9H is also reported in this table. It is no surprise that the B3LYP/TZVP results consistently under estimate the binding energies of the tautomer pair, as Koopmann's theorem is not applicable to Kohn–Sham orbitals directly [32]. As a number of guanine tautomers have been identified in gas phase, the experimental binding energy spectra of guanine needs to be carefully interpreted. Specifically, it must reflect the statistically averaged nature and the contributions from other tautomers. Recent experimental evidence for ionization energies of L-phenylalanine [2], revealed that the first ionization energy of the amino acid was conformer dependent and could range from 8.80 to 9.15 eV. Hence,

Table 3
The outer valence molecular orbital binding energies (ϵ_j in eV), symmetries and pole strengths (in parentheses) for G-7H and G-9H

Molecular	G-7H			G-7H		G-7H		G-7H		G-7H	G-9H			G-9H		G-9H		G-9H	
	OVGF/TZVP (I)			B3LYP/TZVP (I)		SAOP/T2VP (I)		P3[50]		PES	OVGF/TZVP (II)			B3LYP/TZVP (II)		SAOP/T2VP (II)		P3[50]	
Orbital	Symm.	$-\epsilon_j$	PS	Symm.	$-\epsilon_j$	Symm.	$-\epsilon_j$	$-\epsilon_j$	PS	$-\epsilon_j$	Symm.	$-\epsilon_j$	PS	Symm.	$-\epsilon_j$	Symm.	$-\epsilon_j$	$-\epsilon_j$	PS
1	7a″	7.79	(0.90)	7a″	6.06	7a″	9.76	8.27	(0.90)	8.28	7a″	7.69	(0.90)	7a″	5.96	7a″	9.45	8.13	(0.89)
2	6a″	9.64	(0.89)	32a′	7.39	32a′	10.38	9.91	(0.88)	9.90	32a′	9.86	(0.89)	32a′	7.28	32a′	10.45	9.82	(0.88)
3	32a′	9.86	(0.89)	6a″	7.70	6a″	10.81	9.94	(0.88)	9.90	6a″	9.96	(0.89)	31a′	7.56	31a′	10.70	10.02	(0.87)
4	5a″	10.44	(0.88)	31a′	7.80	31a′	10.87	10.27	(0.87)	10.40	31a′	10.25	(0.88)	6a″	7.97	6a″	11.31	10.20	(0.88)
5	31a′	10.53	(0.89)	5a″	8.14	5a″	11.29	10.58	(0.87)	10.40	5a″	10.39	(0.88)	5a″	8.10	5a″	11.35	10.40	(0.87)
6	30a′	11.04	(0.89)	30a′	8.44	30a′	11.61	11.06	(0.87)	11.20	4a″	10.94	(0.88)	4a″	8.80	4a″	11.96	11.12	(0.88)
7	4a″	11.13	(0.88)	4a″	8.97	4a″	12.35	11.24	(0.88)	11.20	30a′	11.41	(0.89)	30a′	8.89	30a′	11.98	11.32	(0.84)
8	29a′	13.50	(0.85)	3a″	10.93	3a″	13.91	13.29	(0.85)	13.00	3a″	13.45	(0.85)	3a″	10.88	3a″	13.85	11.50	(0.88)
9	3a″	14.39	(0.84)	29a′	11.77	29a′	14.59	14.77	(0.87)		2a″	14.36	(0.85)	29a′	11.52	29a′	14.30	14.35	(0.85)
10	2a″	14.71	(0.89)	2a″	11.97	28a′	14.73	14.31	(0.87)		29a′	14.64	(0.89)	2a″	11.92	28a′	14.61	14.50	(0.87)
11	28a′	15.10	(0.88)	28a′	12.11	2a″	14.99	14.91	(0.87)		28a′	14.86	(0.88)	28a′	12.01	2a″	14.84	14.62	(0.87)
12	27a′	15.49	(0.89)	27a′	12.89	27a′	15.43	15.58	(0.88)		27a′	15.38	(0.89)	27a′	12.85	27a′	15.42	15.48	(0.87)
13	26a′	15.70	(0.82)	1a″	13.21	1a″	16.03	15.62	(0.82)		1a″	15.71	(0.83)	1a″	13.20	1a″	15.99	15.71	(0.83)
14	1a″	16.54	(0.88)	26a′	13.68	26a′	16.48				26a′	16.38	(0.88)	26a′	13.56	26a′	16.14		
15	25a′	17.61	(0.89)	25a′	14.44	25a′	17.11				25a′	17.68	(0.89)	25a′	14.51	25a′	17.05		
16	24a′	18.08	(0.87)	24a′	15.20	24a′	17.43				24a′	18.06	(0.87)	24a′	15.18	24a′	17.65		
17	23a′	18.35	(0.87)	23a′	15.39	23a′	18.14				23a′	18.17	(0.87)	23a′	15.28	23a′	17.72		
18				22a′	16.76	22a′	19.28							22a′	16.72	22a′	19.09		
19				21a′	17.14	21a′	19.43							21a′	17.19	21a′	19.67		
20				20a′	18.41									20a′	18.29				
21				19a′	18.53									19a′	18.59				
22				18a′	21.16									18a′	20.95				

(I) Calculation performed at the G-7H (planar) or G-7H B3LYP/TZVP optimised geometry.
(II) Calculation performed at the G-9H (planar) or G-9H B3LYP/TZVP optimised geometry.

experimental binding energies can be only used as a guide for the tautomers under study.

The binding energies generated using the SAOP and the OVGF theory calculations, for the planar guanine tautomers, are in good agreement over most molecular orbitals considered, in particular in the higher energy region. The DFT based SAOP calculations provide reasonable agreement with the experimental measurements, whilst there is excellent agreement observed between experiment and the OVGF theory calculations. The calculated pole strengths (PS) using the OVGF theory are in good agreement with those calculated using the P3 model, with a general trend of PS $\geq$ 0.85. This indicates that the one electron approximation employed in the present work is appropriate. A few MOs in the tautomer pair have orbital pole strengths that are slightly smaller than 0.85. These include orbitals 3a″ and 26a′ in planar G-7H and orbital 1a″ in planar G-9H. In these cases there is a possibility that the one-electron picture may break down.

The good agreement observed between the experimental ionization energies and the theoretically predicted values, together with the geometries discussed earlier, indicate that the planar guanine tautomer bonding might provide valuable insight into the non-planar guanine tautomers, for at least the purine ring. An energy level diagram based on the B3LYP/TZVP orbital energies for the planar guanine tautomer pair, is presented in Fig. 3. Here the molecular orbital correlations are shown between the respective tautomers. As found in adenine [22], protons do not possess cores so that the proton transfer does not cause any fundamental changes in the geometries and does not affect the ordering of the highest occupied molecular orbital (HOMO) and next HOMO (NHOMO) [22]. Therefore, we reiterate that in the study of tautomer changes it is important to consider the full spectrum of the valence space, rather than only focus on the frontier MOs. Fig. 3 indicates the orbital energy alternations (energy shifts and level crossings) as a result of the proton transfer in the guanine keto pair. Here the tautomer pair has been treated as planar species, so that the valence orbitals are divided into two irreducible representations: one with orbitals of a′ symmetry which are symmetric with respect to the plane reflection and which are likely to form in-plane σ bonds; the other has orbitals of a″ symmetry which are anti-symmetric with respect to the plane reflection and which are likely to form out-of-plane π bonds. A hydrogen atom typically has only occupied 1s orbitals, therefore it is expected that the mobile proton has limited influence on the out-of-plane π bonding. This point has also been revealed in other planar DNA base studies [22,53]. The proton effects on the a″ orbitals can only be indirectly inferred through affecting the energies of the related a′ orbitals, thereby causing an energy shift or orbital crossing which is in fact the case as shown in Fig. 3. It is also seen from this figure that although the mobile proton causes greater or smaller energy shifts throughout the entire valence region ϵ_j<20 eV, its most substantial influence is on the orbitals in the energy region ϵ_j=9–12 eV.

3.4. Orbitals and their momentum distributions

To understand the details of the energy patterns in Fig. 3, for the guanine tautomer pair, the orbital wave functions need to be

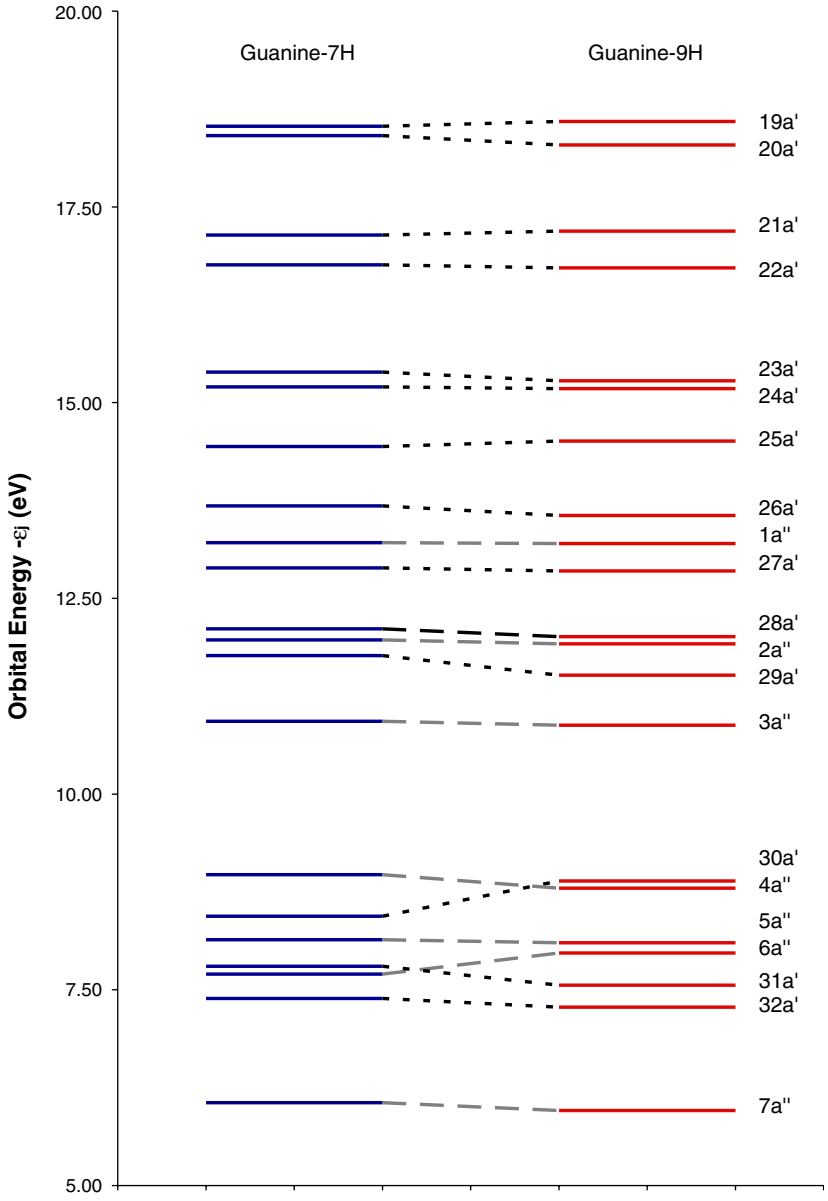

Fig. 3. The G-7H (planar) and G-9H (planar) tautomer outer valence molecular orbital energies as calculated using B3LYP/TZVP, for the B3LYP/TZVP optimized geometry. The grey/dash lines correlate the anti-symmetry MOs (a″); The black/dot dash lines correlate the symmetric MOs (a′).

closely inspected. To this end, dual space analysis [28] is now employed. Orbital momentum distributions (MDs) for the outer valence region of both the planar G-7H and G-9H tautomers have been calculated and screened, on an orbital by orbital basis, in the region of $\epsilon_j < 20$ eV. These orbitals are in general divided into three groups, depending on the degree of the tautomeric related changes: the orbitals in group one harbor little change; orbitals in group two exhibit noticeable (but small) changes and the orbitals in group three demonstrate significant changes and therefore are the signature orbitals of the keto tautomeric changes between G-7H/G-9H.

As expected from their symmetry, the group one orbitals consist largely of a″ orbitals, i.e., 1a″, 2a″, 3a″, 4a″, 5a″, 6a″ and 7a″, although there are some orbitals of a′ symmetry such as 18a′. We note that the latter orbitals of a′ symmetry are closer to the inner valence region, which is away from the mobile proton affected region. Some of the a″ orbitals in this group, such as the 7a″ HOMO, exhibit small discrepancies in their MDs between the G-7H and G-9H tautomers in the low momentum region. Fig. 4 uses the 7a″ and 1a″ orbitals as representative group I exemplars. In this figure we show the Dyson orbital MDs (middle column) and position space charge distributions for both orbitals of both tautomers. Fig. 4(b) clearly indicates the *p* electron domination of the 7a″ MO in both tautomers, as the orbital MDs have a Gaussian-like distribution in momentum space. It is further noted from the orbital electron charge densities in Fig. 4(a) and (c), that in position space the HOMOs (7a″) are typical *p*-electron dominant orbitals for the G-7H and G-9H tautomers (as anti-bonding π orbitals). This anti-bonding nature of the HOMOs represent a more localized $2p_z$ atomic orbital (AO) contribution from the "heavy" atoms such as C, O and N in guanine. The

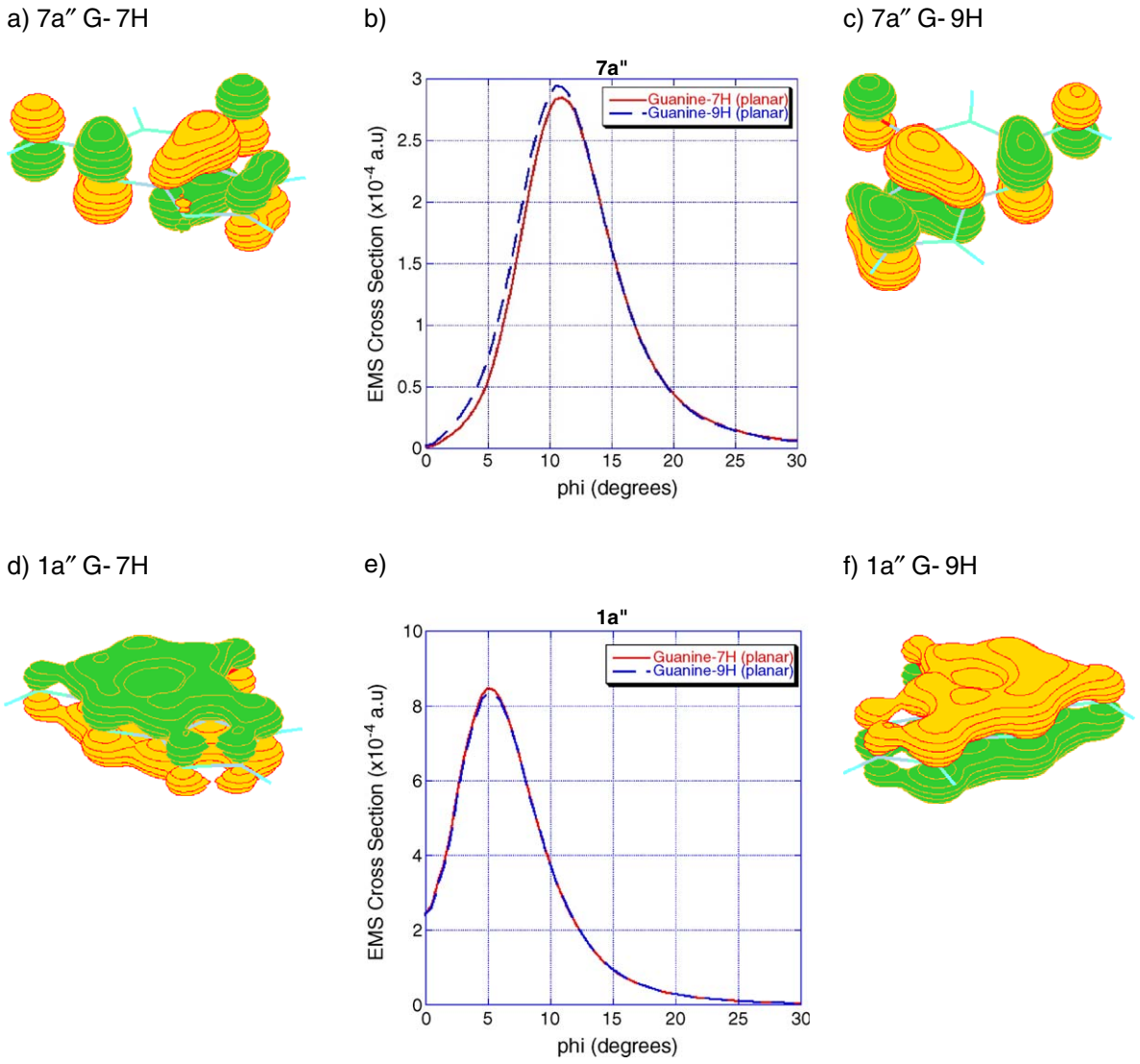

Fig. 4. The G-7H and G-9H tautomer 7a″ and 1a″ orbital MDs are shown together with the corresponding orbital diagrams. These orbitals represent examples of the group I orbitals. The orbital diagrams for the tautomers are plotted using Molden [56].

MDs of the 1a″ orbital are also *p*-electron dominant, but with a "missing" lower momentum part of the Gaussian-like distribution. This is an indication of a delocalized (bonding) π orbital (no sign changes in the same side of the molecular plane). The Dyson orbital charge distributions of the 1a″ orbitals, as shown in Fig. 4(d) and (f), confirm the important π-bonding nature observed from the information in momentum space.

The other two groups of orbitals are likely to be those orbitals within the molecular plane, and we now discuss (in turn) each of these groups. Orbitals in group two are those which receive some perturbation as a result of the mobile proton transfer. However, in this case such perturbations distort the orbital wave functions without significantly changing the nature of the bonding. These are the 19a′–22a′, 25a′, 26a′, 28a′, 29a′ and 31a′ orbitals. The shapes of the orbital MDs in this group indicate that the orbitals are largely dominated by $s^x p^y$ hybridization, where x and y indicate the degree of s or p bonding which is orbital dependent. Fig. 5 illustrates the 20a′ and 31a′ Dyson orbitals in coordinate and momentum spaces for the guanine pair. Considering orbital 20a′ first, the MDs (Fig. 5(b)) indicate strong s and p bonding with a "local minimum" at approximately 5° for both G-7G and G-9H. This observation implies a separation of two intensive electron charge density distributions. Inspection of the Dyson orbitals in coordinate space indicates that the two dimensional (2D) electron charge distribution of G-7H is concentrated on the hexagon chain of $H–N_{(1)}–C_{(2)}–N_{(3)}–C_{(4)}$. This includes the $C_{(2)}–N_{(2)}H_{(21)}$ side chain, which is separated from the electron density formed by $C_{(8)}–N_{(7)}–H$ (Fig. 5(a)). On the other hand, in the G-9H tautomer the smaller electron density is replaced by the chain of $H–C_{(8)}–N_{(7)}$, which is again well separated from the electron cloud formed by the atoms in the hexagonal ring (Fig. 5(c)). However, it is interesting to note that in G-9H the hydrogen atom in the shorter chain is not from the mobile hydrogen on the $N_{(9)}$ atom, but from the hydrogen bonded with $C_{(8)}$ instead. Orbital 31a′ in G-7H is a strong *s*-electron dominant orbital (Fig. 5(e)), largely contributed to by the lone

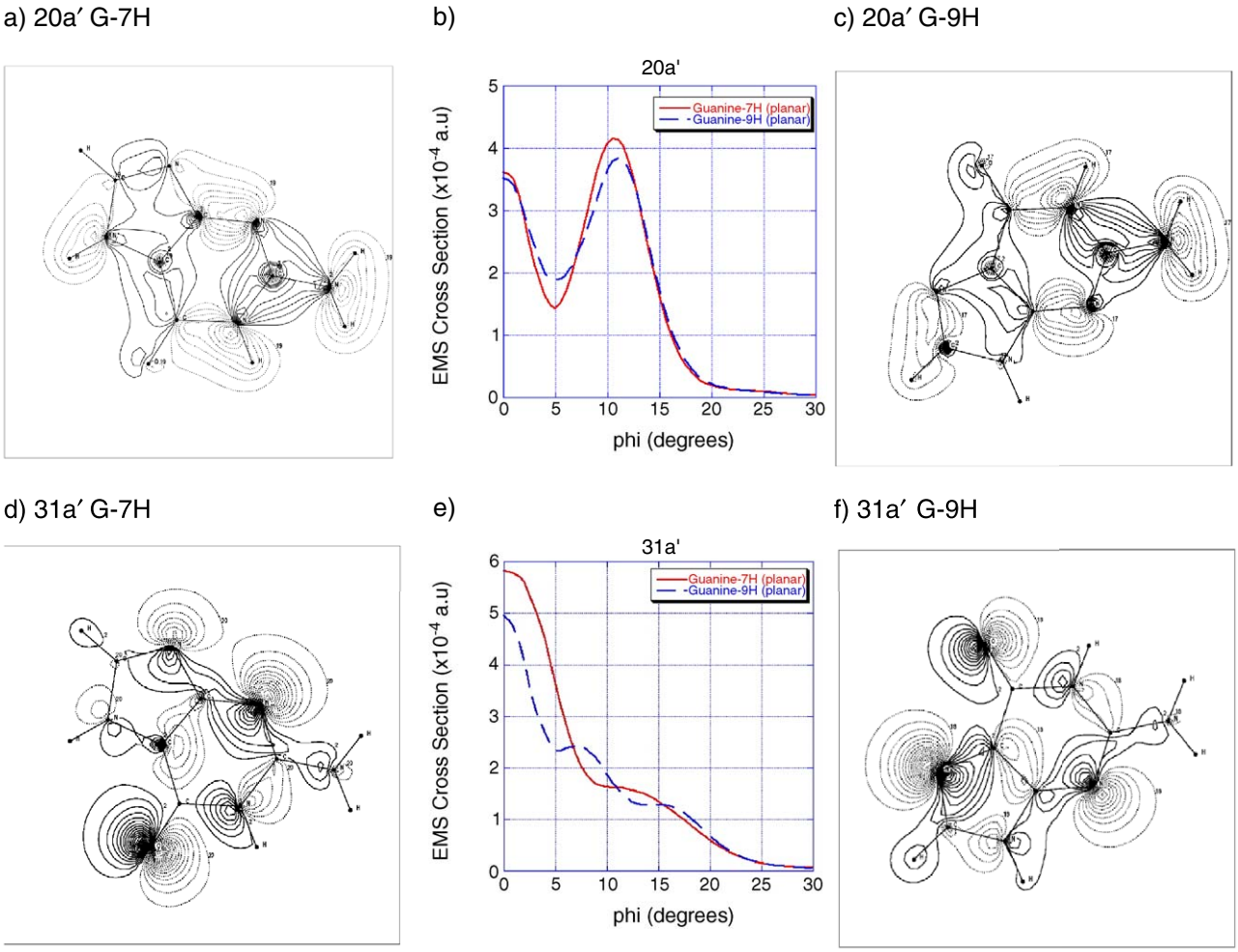

Fig. 5. The G-7H and G-9H tautomer 31a′ and 20a′ orbital MDs are shown together with the corresponding orbital diagrams. These orbitals represent examples of the group II orbitals. The orbital diagrams for the tautomers are plotted using Molden [56].

pairs located on the oxygen of the C═O group as well as by the lone electron pairs located on $N_{(3)}$ and $N_{(9)}$ (Fig. 5(d)). In the G-9H case, an analogous electron density pattern is observed. However, the lone electron pair is now located on $N_{(7)}$ instead of on $N_{(9)}$ (Fig. 5(f)).

The third group of orbitals demonstrate the most significant alternations between the G-7H and G-9H tautomers due to the mobile proton transfer. They are identified as orbitals 23a′, 24a′, 27a′, 30a′ and 32a′, with Fig. 6 displaying their orbital MDs. As found in the adenine A-9H/A-7H tautomers [22], the mobile proton signatures of the tautomers become more apparent in the mid- to low-momentum region. Two of the five group three orbitals, i.e. 30a′ and 32a′, do not in fact exhibit significant changes in their nature. Namely, while the G-9H and G-7H MDs for the respective 30a′ and 32′ orbitals are clearly different, the component atoms which contribute to the bonding mechanisms are identical. Here the differences arise from enhanced *s* contributions, caused by the ability for the "bare" nitrogen ($N_{(7)}$ or $N_{(9)}$) electron density to partially overlap with that of the oxygen atom in the 30a′ orbital in G-9H, and the combined contributions from $C_{(4)}$ and $N_{(3)}$ for orbital 32a′ in G-7H. However, orbitals 23a′, 24a′ and 27a′ experience significant changes in their orbital MDs and in their bonding nature, as we now discuss in detail. To further explore the electronic information guided by the orbital MDs, Fig. 7 reports the dual space orbital information, i.e. information from both coordinate and momentum spaces for orbitals 23a′ and 24a′. Orbital 23a′ of G-7H receives contributions from all the N–H and C–H bonds (Fig. 7(a)), so that its orbital MD exhibits a strong s component (Fig. 7(b)). Moreover, the bonding nature of $N_{(1)}$–H and $N_{(2)}$–$H_{(21)}$ enhances the s character observed in this orbital. For G-9H, on the other hand, not all the N–H and C–H bonds are involved in the bonding (Fig. 7(c)). For example, the $N_{(9)}$–H and $N_{(1)}$–H bonds are not intensively populated (Fig. 7(c)), which leads to the reduced s character observed for this orbital. Similarly, orbital 24a′ of G-7H shows a stronger *s* character than its G-9H counterpart, although its mobile hydrogen bond $N_{(7)}$–H is less populated. The G-9H counterpart of this orbital (Fig. 7(f)) is more populated by electron charges from almost all the atoms, although its anti-bonding nature prevents this orbital from having a strong *s*-like contribution (Fig. 7(e)). It is noted from this orbital pair that the contribution from the amine group (–NH_2) is very different in each case: the electron

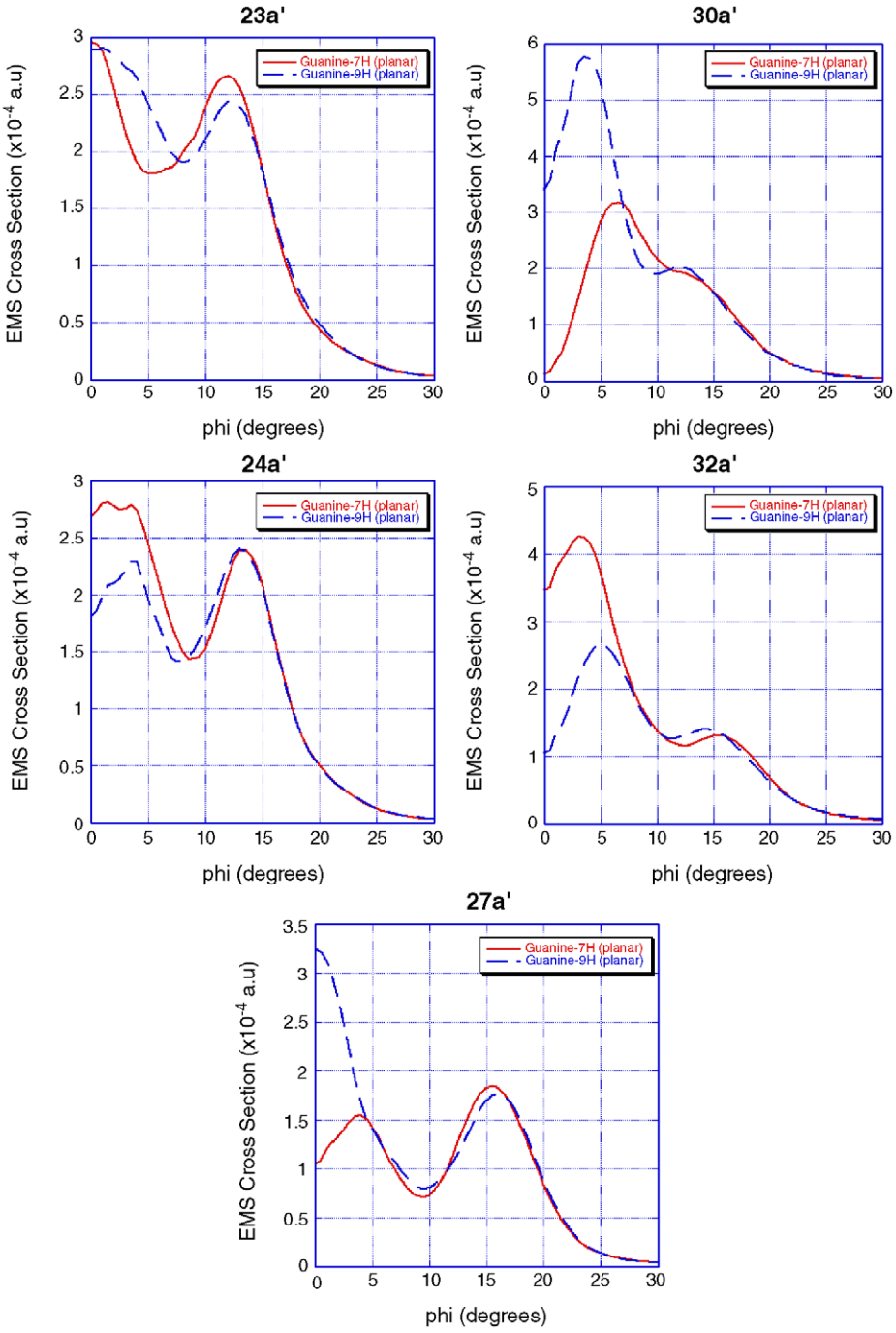

Fig. 6. The G-7H and G-9H tautomer signature MDs (group III), mapped from the B3LYP/TZVP orbital wave functions.

cloud of the N–H pair in G-7H is nearly symmetric and the $N_{(1)}$–H bond interacts with the electrons from the $C_{(2)}$–$N_{(2)}$ bond, whereas in G-9H the amine group contribution is quite asymmetric, and the $N_{(1)}$–H bond interacts with the $-NH_2$ group (Fig. 7(f)), rather than the $C_{(2)}$–$N_{(2)}$ bond.

Fig. 8 gives the last orbital pair from group 3, namely for orbital 27a′. The orbital MDs of this orbital pair (Fig. 8(b)) demonstrate a $s^x p^y$-hybridization nature. Large discrepancies between the tautomers exist in the low momentum region, in particular in the region of $\phi < 5°$. Here G-9H displays a strong *s*-like contribution, in the long range region, that is approximately four times stronger than that observed in the G-7H counterpart. The orbital of G-9H, as given in Fig. 8(c), indicates a very strong negative charge cloud formed by the lone pair of the oxygen of the C═O group, in the hexagon, joining with the lone pair electrons of $N_{(7)}$ on the pentagonal ring. In G-7H, however, the lone pair of electrons in the oxygen of C═O is more isolated, since the $N_{(7)}$ site bonding on H in G-7H is no longer an electron donor in this case. Instead the lone pair electrons located on $N_{(3)}$ in the hexagonal ring and $N_{(9)}$ in the pentagonal ring, contribute to form the negatively charged cloud in G-7H as shown in Fig. 8(a).

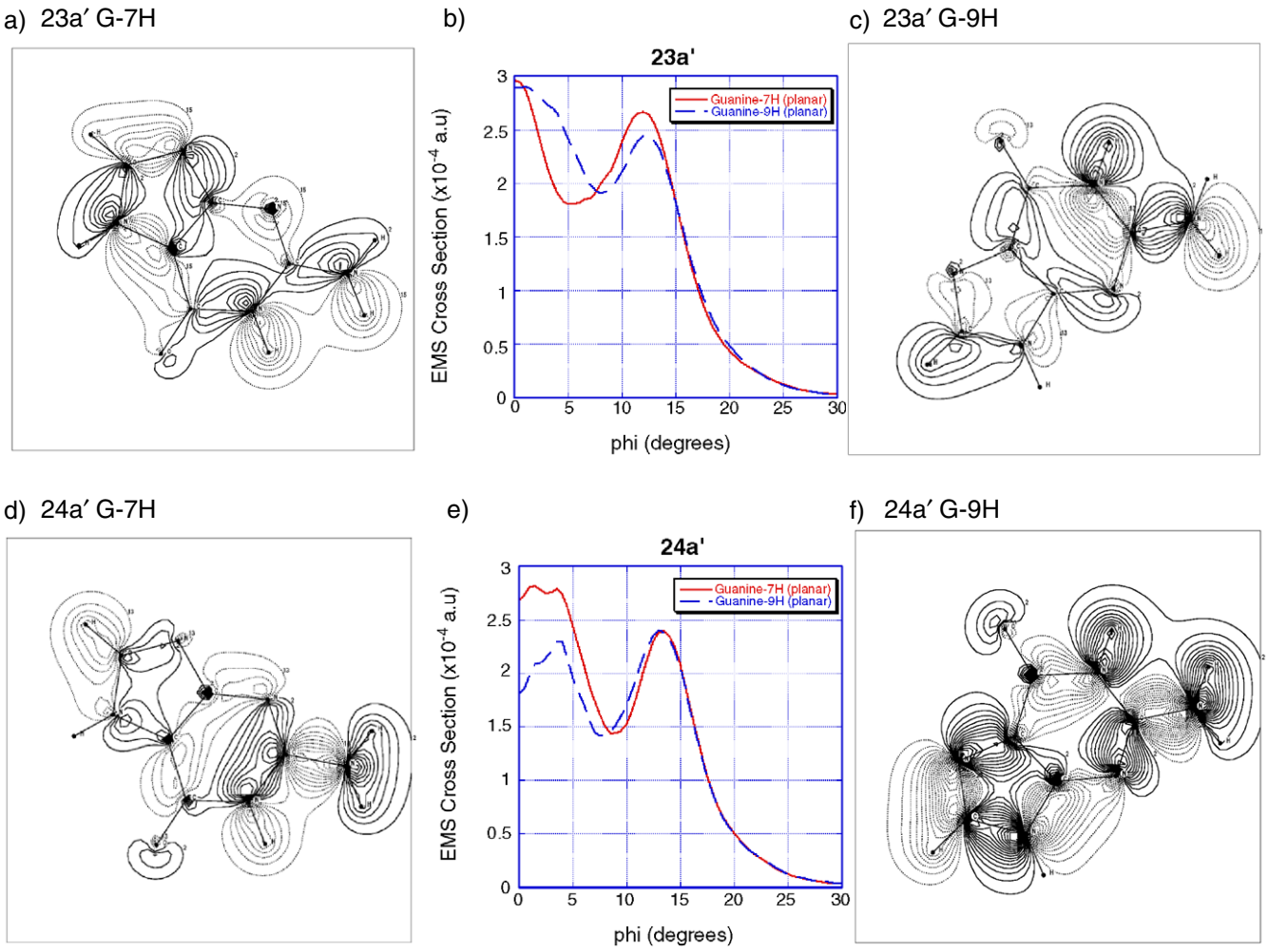

Fig. 7. The G-7H and G-9H tautomer 23a′ and 24a′ orbital MDs are shown together with the corresponding orbital diagrams. These orbitals represent examples of the group III orbitals. The orbital diagrams for the tautomers are plotted using Molden [56].

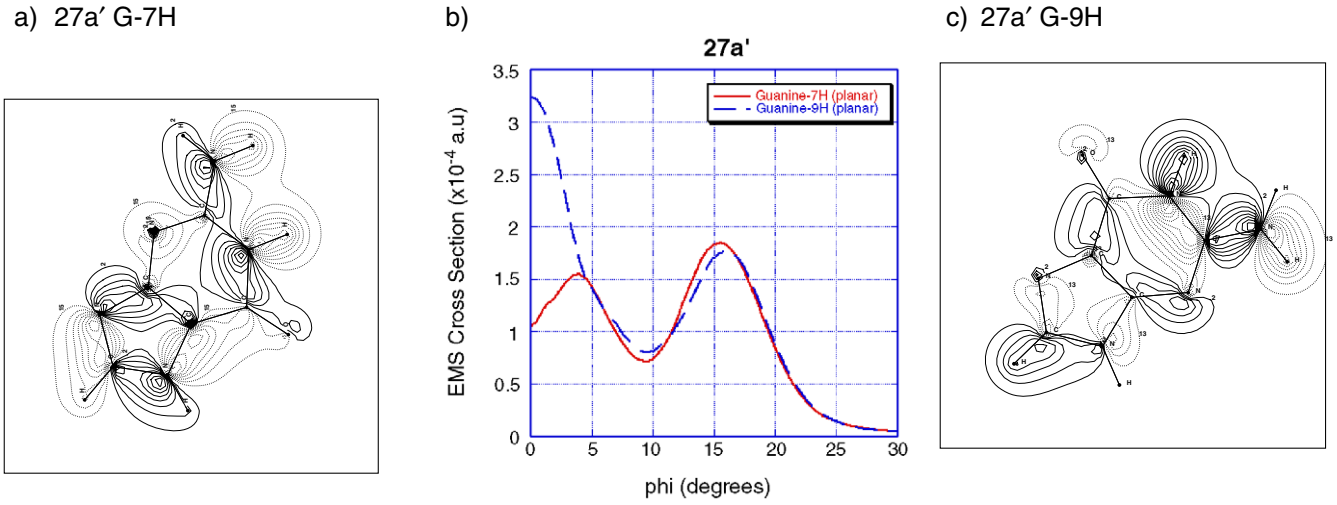

Fig. 8. The G-7H and G-9H tautomer 27a′ orbital MDs are shown together with the corresponding orbital diagrams. This orbital represents an example of the group III orbitals. The orbital diagrams for the tautomers are plotted using Molden [56].

4. Conclusions

The two most stable guanine tautomers have been studied using a combination of density functional and Green's function theory methods. These calculations were combined with the dual space analysis technique to provide additional information into the bonding mechanisms, within the individual species, and to identify orbital based signatures which are sensitive to the proton transfer within the molecule. New orbital binding energies have been calculated using the recently developed SAOP and OVGF theories, and were in good accord with the existing experimental measurements and previous calculations. Our results indicated that the orbital ordering is sensitive to the proton transfer involved in the tautomerism of guanine.

The mobile proton contributes significantly to the distortion of the electron distribution in the molecule. Such distortions are largely orbital based and have been detected in momentum space. The reaction to the tautomeric changes of the valence orbitals in the guanine keto G-7H/G-9H pair can be divided into three groups: (i) Group one orbitals which are almost identical in G-7H and G-9H, indicating they are either out of plane orbitals such as π orbitals, or the orbitals are dominated by contributions from atoms which are far away from the mobile proton location in the molecules. (ii) Group two orbitals which show small perturbations due to the tautomeric process. This includes in-plane σ bonds or the atoms involved in the bonding are in the vicinity of the mobile proton location. (iii) Group three orbitals which are identified in momentum space as tautomer signature orbitals and which experience significant changes between the G-7H and G-9H tautomers. Such group three signature orbitals are dominated by in-plane orbitals with σ bonds, and usually involve the component atoms which are directly interacting with the mobile proton via either through-bond or through-space processes.

We also found that the tautomeric changes may exhibit a significant impact on anisotropic properties such as dipole moments and molecular electrostatic potentials, which are sensitive to the distortion of the electron charge distributions caused by the mobile proton location. The ionization energy spectra of the tautomer pair are also sensitive to the tautomerism, but the experimental observation of tautomer dependent ionization energies requires a future generation of powerful lasers. However, orbitals of the tautomer pair (as noted above for group 3 orbitals) do demonstrate a promising potential signature due to the impact from the mobile proton. Here, the orbital signatures for the G-7G/G-9H tautomeric process were identified in the present study as orbitals 23a′, 24a′, 27a′, 30a′ and 32a′. Finally, the present study demonstrated that the frontier orbitals are not always involved in all the chemical reactions, with the orbital response to a particular chemical process depending on which atoms are contributing to the formation of bonds.

Acknowledgments

This work is supported by the Australian Research Council (ARC). The authors acknowledge the Australian Partnership for Advanced Computing (APAC) for the use of the National Supercomputing Facilities. DBJ also thanks the Ferry Trust and the Complex System Sciences group of the CSIRO for financial support.

Appendix A. Supplementary data

Supplementary data associated with this article can be found, in the online version at doi:10.1016/j.bpc.2005.12.006.

References

[1] K.T. Lee, J. Sung, K.J. Lee, Y.D. Park, S.K. Kim, Conformation-dependent ionization energies of L-phenylalanine, Angew, Chem. Int. Ed. 41 (2002) 4114.
[2] K.T. Lee, J. Sung, K.J. Lee, S.K. Kim, Y.D. Park, Conformation-dependent ionization of L-phenylalanine: structures and energetics of cationic conformers, Chem. Phys. Lett. 368 (2003) 262.
[3] E.G. Robertson, R.J.S. Morrison, Gas phase conformation in the ibuprofen analogues isobutylbenzene and 2-phenylpropionic acid, Mol. Phys. 103 (2005) 1625.
[4] J.J. Neville, Y. Zheng, C.E. Brion, Glycine valence orbital electron densities: comparison of electron momentum spectroscopy experiments with Hartree–Fock and density functional theories, J. Am. Chem. Soc. 118 (1995) 10533.
[5] J. Elguero, A.R. Katrizky, O.V. Denisko, in: A.R. Katrizky (Ed.), Advances in Heterocyclic Chemistry, vol. 76, Academic Press, New York, 2000.
[6] M.K. Shukla, S.K. Mishra, A. Kumar, P.C. Mishra, An ab initio study of excited states of guanine in the gas phase and aqueous media: electronic transitions and mechanisms of spectral oscillations, J. Comput. Chem. 21 (2000) 826.
[7] M. Sabio, S. Topiol, W.C.L. Jr., An investigation of tautomerism in adenine and guanine, J. Phys. Chem. 94 (1990) 1366.
[8] M. Hanus, F. Ryjacek, M. Kabelac, T. Kubar, T.V. Bogdan, S.A. Trygubenko, P. Hobza, Correlated ab initio study of nucleic acid bases and their tautomers in the gas phase, in a microhydrated environment and in aqueous solution. Guanine: surprising stabilization of rare tautomers in aqueous solution, J. Am. Chem. Soc. 125 (2003) 7678.
[9] M. Haranczyk, M. Gutowski, Valence and dipole-bound anions of the most stable tautomers of guanine, J. Am. Chem. Soc. 127 (2005) 699.
[10] M. Haranczyk, M. Gutowski, Finding adiabatically bound anions of guanine through a combinatorial computational approach, Angew, Chem. Int. Ed. 44 (2005) 6585.
[11] X. Yang, X.B. Wang, E.R. Vorpagel, L.S. Wang, Direct experimental observation of the low ionization potentials of guanine in free oligonucleotides by using photoelectron spectroscopy, PNAS 101 (2004) 17588.
[12] M. Piacenza, S. Grimme, Systematic quantum chemical study of DNA-base tautomers, J. Comput. Chem. 25 (2004) 83.
[13] B. Giese, D. McNaughton, Density functional theoretical (DFT) and surface enhanced Raman spectroscopic study of guanine and its alkylated derivatives: Part 1. DFT calculations on neutral, protonated and deprotonated guanine, Phys. Chem. Chem. Phys. 4 (2002) 5161.
[14] W. Chin, M. Mons, I. Dimicoli, F. Piuzzi, B. Tardivel, M. Elhanine, Tautomer contribution's to the near UV spectrum of guanine: towards a refined picture for the spectroscopy of purine molecules, Eur. Phys. J., D At. Mol. Opt. Phys. 20 (2002) 347.
[15] E. Nir, C. Janzen, P. Imhof, K. Kleinermanns, M.S. de Vries, Guanine tautomerism revealed by UV–UV and IR–UV hole burning spectroscopy, J. Chem. Phys. 115 (2001) 4604.
[16] J. Lin, C. Yu, S. Peng, I. Akiyama, K. Li, L.K. Lee, P.R. LeBreton, Ultraviolet photoelectron studies of the ground-state electronic structure and gas-phase tautomerism of hypoxanthine and guanine, J. Phys. Chem. 84 (1980) 1006.
[17] P.R. LeBreton, X. Yang, S. Urano, S. Fetzer, M. Yu, N.J. Leonard, S. Kumar, Photoemission properties of methyl-substituted guanines:

photoelectron and fluorescence investigations of 1,9-dimethylguanine, 0^6,9-dimethylguanine, and 9-methylguanine, J. Am. Chem. Soc. 112 (1990) 2138.
[18] J. Leszczynski, The potential energy surface of guanine is not flat: an ab initio study with large basis sets and higher order electron correlation contributions, J. Phys. Chem., A 102 (1998) 2357.
[19] J. Sponer, P. Hobza, Non-planar geometries of DNA bases. Ab initio secondorder Møller–Plesset study, J. Phys. Chem. 98 (1994) 3161.
[20] C. Colominas, F.J. Luque, M. Orozco, Tautomerism and protenation of guanine and cytosine. Implications in the formation of hydrogen-bonded complexes, J. Am. Chem. Soc. 118 (1996) 6811.
[21] C.F. Guerra, F.M. Bickelhaupt, S. Saha, F. Wang, Adenine tautomers: relative stabilities, ionization energies and mismatch with cytosine, J. Phys. Chem., A (submitted for publication).
[22] F. Wang, M.T. Downton, N. Kidwani, Adenine tautomer electronic structural signatures studied using dual space analysis, J. Theo. Comp. Chem. 4 (2005) 247.
[23] F. Wang, Assessment of quantum mechanical models based on resolved orbital momentum distributions of *n*-butane in the outer valence shell, J. Phys. Chem., A 107 (2003) 10199.
[24] A.D. Becke, Density-functional thermochemistry: III. The role of exact exchange, J. Chem. Phys. 98 (1993) 5648.
[25] C. Lee, W. Yang, R.G. Parr, Development of the Colle–Salvetti correlation energy formula into a functional of the electron density, Phys. Rev., B 37 (1988) 785.
[26] N. Godbout, D.R. Salahub, J. Andzelm, E. Wimmer, Optimization of Gaussian type basis sets for local spin density functional calculations: Part I. Boron through neon, optimization technique and validation, Can. J. Chem. 70 (1992) 560.
[27] M.J. Frisch, G.W. Trucks, H.B. Schlegel, G.E. Scuseria, M.A. Robb, J.R. Cheeseman, J.A. Montgomery, Jr., T. Vreven, K.N. Kudin, J.C. Burant, J. M. Millam, S.S. Iyengar, J. Tomasi, V. Barone, B. Mennucci, M. Cossi, G. Scalmani, N. Rega, G.A. Petersson, H. Nakatsuji, M. Hada, M. Ehara, K. Toyota, R. Fukuda, J. Hasegawa, M. Ishida, T. Nakajima, Y. Honda, O. Kitao, H. Nakai, M. Klene, X. Li, J.E. Knox, H.P. Hratchian, J.B. Cross, V. Bakken, C. Adamo, J. Jaramillo, R. Gomperts, R.E. Stratmann, O. Yazyev, A.J. Austin, R. Cammi, C. Pomelli, J.W. Ochterski, P.Y. Ayala, K. Morokuma, G.A. Voth, P. Salvador, J.J. Dannenberg, V.G. Zakrzewski, S. Dapprich, A.D. Daniels, M.C. Strain, O. Farkas, D.K. Malick, A.D. Rabuck, K. Raghavachari, J.B. Foresman, J.V. Ortiz, Q. Cui, A.G. Baboul, S. Clifford, J. Cioslowski, B.B. Stefanov, G. Liu, A. Liashenko, P. Piskorz, I. Komaromi, R.L. Martin, D.J. Fox, T. Keith, M.A. Al-Laham, C.Y. Peng, A. Nanayakkara, M. Challacombe, P.M.W. Gill, B. Johnson, W. Chen, M. W. Wong, C. Gonzalez, J.A. Pople, Gaussian 03, Revision C. 02, Gaussian, Inc., Wallingford, CT, 2004.
[28] F. Wang, M.J. Brunger, I.E. McCarthy, D.A. Winkler, Exploring the electronic structure of 2,6-stelladione from momentum space: I. The p-dominant molecular orbitals in the outer valence shell, Chem. Phys. Lett. 382 (2003) 217.
[29] F. Wang, M.J. Brunger, D.A. Winkler, Structural impact on the methano bridge in norbornadiene, norbornene and norbornane, J. Phys. Chem. Solids 65 (2004) 2041.
[30] M.T. Downton, F. Wang, Chemical bonding mechanisms of *n*-butane probed by the core orbitals of conformational isomers in r-space and k-space, Chem. Phys. Lett. 384 (2004) 144.
[31] K.L. Nixon, F. Wang, L. Campbell, T. Maddern, D.A. Winkler, R. Gleiter, P. Loeb, E. Weigold, M.J. Brunger, An electron momentum spectroscopy and density functional theory study of the outer valence electronic structure of stella-2,6-dione, J. Phys., B At. Mol. Opt. Phys. 36 (2003) 3155.
[32] T. Koopmans, Ordering of wave functions and eigenvalues to the individual electrons of an atom, Physica (Amsterdam) 1 (1933) 104.
[33] W. von Niessen, J. Schirmer, L.S. Cederbaum, Computational methods for the one-particle green's function, Comput. Phys. Rep. 1 (1984) 57.
[34] L.S. Cederbaum, W. Domcke, Theoretical aspects of ionization potentials and photoelectron spectroscopy: a green's function approach, Adv. Chem. Phys. 36 (1977) 205.
[35] O.V. Gritsenko, R. van Leeuwen, E.J. Baerends, Analysis of electron interaction and atomic shell structure in terms of local potentials, J. Chem. Phys. 101 (1994) 8955.
[36] O.V. Gritsenko, R. van Leeuwen, E.J. Baerends, Molecular Kohn–Sham exchange-correlation potential from the correlated ab initio electron density, Phys. Rev., A 52 (1995) 1870.
[37] O.V. Gritsenko, P.R.T. Schipper, E.J. Baerends, Approximation of the exchange-correlation Kohn–Sham potential with a statistical average of different orbital model potentials, Chem. Phys. Lett. 302 (1999) 199.
[38] S. Knippenberg, K.L. Nixon, M.J. Brunger, T. Maddern, L. Campbell, N. Trout, F. Wang, W.R. Newell, M.S. Deleuze, J.P. Francois, D.A. Winkler, Norbornane: an investigation into its valence electronic structure using electron momentum spectroscopy, and density functional and Green's function theories, J. Chem. Phys. 121 (2004) 10525.
[39] S. Knippenberg, K.L. Nixon, H. Mackenzie-Ross, M.J. Brunger, F. Wang, M.S. Deleuze, J.-P. Francois, D.A. Winkler, An investigation into the valence electronic structure of norbornene using electron momentum spectroscopy, Green's function and density functional theories, J. Phys. Chem., A 109 (2005) 9324.
[40] E.J. Baerends, J. Autschbach, A. Bérces, C. Bo, P.M. Boerrigter, L. Cavallo, D.P. Chong, L. Deng, R.M. Dickson, D.E. Ellis, L. Fan, T.H. Fischer, C.F. Guerra, S.J.A. van Gisbergen, J.A. Groeneveld, O.V. Gritsenko, M. Grüning, F.E. Harris, P. van den Hoek, H. Jacobsen, G. van Kessel, F. Kootstra, E. van Lenthe, V.P. Osinga, S. Patchkovskii, P.H.T. Philipsen, D. Post, C.C. Pye, W. Ravenek, P. Ros, P.R.T. Schipper, G. Schreckenbach, J.G. Snijders, M. Sola, M. Swart, D. Swerhone, G. te Velde, P. Vernooijs, L. Versluis, O. Visser, E. van Wezenbeek, G. Wiesenekker, S.K. Wolff, T.K. Woo, T. Ziegler, ADF version 03, http://www.scm.com (2002).
[41] D.P. Chong, E. van Lenthe, S. van Gisbergen, E.J. Baerends, Even-tempered slater-type orbitals revisited: from hydrogen to krypton, J. Comput. Chem. 25 (2004) 1030.
[42] E. Weigold, I.E. McCarthy, Electron Momentum Spectroscopy, Kluwer Academic/Plenum Publishers, NY, 1999.
[43] I.E. McCarthy, E. Weigold, Electron momentum spectroscopy of atoms and molecules, Rep. Prog. Phys. 54 (1991) 789.
[44] M.J. Brunger, W. Adcock, High-resolution electron momentum spectroscopy of molecules, J. Chem. Soc., Perkin Trans. 2 (2002) 1.
[45] Y. Khajuria, M. Takahashi, Y. Udagawa, Electron momentum spectroscopy of N_2O, J. Electron Spectrosc. Relat. Phenom. 133 (2003) 113.
[46] S.I. Kawahara, T. Uchimaru, Second order many-body perturbation approximations to the coupled cluster Greens function, J. Chem. Phys. 102 (1995) 1681.
[47] T.-K. Ha, H.-J. Kellar, R. Gunde, H.-H. Gunthard, Energy increment method based on quantum chemical results: a general recipe for approximative prediction of isomerization and tautomerization energies of pyrimidine and purine nucleic acid bases and related compounds, J. Phys. Chem., A 103 (1999) 6612.
[48] M. Feyereisen, G. Fitzgerald, A. Komornicki, Use of approximate integrals in ab initio theory. An application in MP2 energy calculations, Chem. Phys. Lett. 208 (1993) 359.
[49] G.G. Sheina, S.G. Stepanian, E.D. Radchenko, Y.P. Blagio, IR spectra of guanine and hypoxanthine isolated molecules, J. Mol. Struct. 158 (1987) 275.
[50] O. Dolgounitcheva, V.G. Zakrzewski, J.V. Ortiz, Electron propagator theory of guanine and its cations: tautomerism and photoelectron spectra, J. Am. Chem. Soc 122 (2000) 12304.
[51] S.I. Kawahara, T. Uchimaru, Basis set effect on hydrogen bond stabilization energy estimation of the Watson–Crick type nucleic acid base pairs using medium-size basis sets: single point MP2 evaluations at the HF optimized structures, Phys. Chem. Chem. Phys. 2 (2000) 2869.
[52] L. Clowney, S.C. Jain, A.R. Srinivasan, J. Westbrook, W.K. Olson, H.M. Berman, Geometric parameters in nucleic acids: nitrogenous bases, J. Am. Chem. Soc. 118 (1996) 509.
[53] S. Saha, F. Wang, C.T. Falzon, M.J. Brunger, Co-existence of 1,3-butadiene conformers in ionization energies and Dyson orbitals, J. Chem. Phys. 123 (2005) 124315.

[54] D.B. Pedersen, B. Simard, A. Martinez, A. Moussatova, Stabilization of an unusual tautomer of guanine: photoionization of al-guanine and al-guanine-$(NH_3)_n$, J. Phys. Chem., A 107 (2003) 6464.
[55] T. Melvin, M.A. Plumb, S.W. Botchway, P. O'Neill, A.W. Parker, 193 nm light induces single-strand breakage of DNA predominantly at guanine, Photochem. Photobiol. 61 (1995) 584.
[56] G. Schaftenaar, J. Noordik, Molden: a pre- and post-processing program for molecular and electronic structures, J. Comput.-Aided Mol. Des. 14 (2000) 123.
[57] B. Mennucci, A. Toniolo, J. Tomasi, Theoretical study of guanine from gas phase to aqueous solution: role of tautomerism and its implications in absorption and emission spectra. J. Phys. Chem., A 105 (2001) 7126.